Contribution from the Department of Chemistry, University of Missouri—Rolla, Rolla, Missouri 65401, Atomic Energy Research Establishment, Harwell, Didcot, 0X11 ORA England, and Institut de Physique, Université de Liège, B-4000 Sart-Tilman, Belgium

Iron-57 and Antimony-121 Mössbauer-Effect Study of Several Spinel Antimonates

FERNANDE GRANDJEAN, GARY J. LONG,* GEOFFREY LONGWORTH, and BRIAN J. LAUNDY

Received May 25, 1983

The iron-57 and antimony-121 Mössbauer-effect spectra of six iron-containing antimonate spinels, of general formula $M^{II}_{12}Fe^{III}_{3}Sb^{V}_{3}O_{24}$, where M^{II} is divalent zinc, magnesium, cobalt, and nickel, and the spinel $Ni_{10}Fe_6Sb_2O_{24}$ have been measured and the 4.2 K iron-57 results used to determine the cation distribution between the tetrahedral A and the octahedral B sites. If M^{II} is diamagnetic zinc(II), all the iron(III) is located on the octahedral B site and the ordering temperature is ca. 1.35 K. In the orthorhombic spinel $Mg_{12}Fe_3Sb_3O_{24}$, two-thirds of the iron is on the tetrahedral A site and the ordering temperature is ca. 5 K. When M^{II} is nickel(II) and either cobalt(II) or magnesium(II), there is a distinct preference for the nickel(II) to occupy the octahedral B site and, in so doing, to displace some additional iron(III) from these sites onto the tetrahedral A sites. The presence of magnetic cobalt(II) and nickel(II) cations increases the ordering temperature to ca. 200 K in these compounds. In each case the room-temperature spectra show lines corresponding to both tetrahedral and octahedral iron(III) quadrupole-split doublets with typical hyperfine parameters. Below the ordering temperature, each compound shows at least two iron-57 Mössbauer-effect magnetic sextets with hyperfine fields at 4.2 K of ca. 450 kOe for the tetrahedral site and ca. 530 kOe for the octahedral site. In several instances, a small distribution in the hyperfine field is observed and attributed to the distribution of the cations on the near-neighbor sites. In each compound a few area percent of a paramagnetic impurity is observed in the magnetic spectra, and the nature of this impurity is discussed. The room-temperature antimony-121 Mössbauer spectra of these materials show an isomer shift typical of antimony(V) and no hyperfine field at the antimony nucleus. Similar results are obtained for $Zn_{12}Fe_3Sb_3O_{24}$ and $Mg_{12}Fe_3Sb_3O_{24}$ at 4.2 K. However, the compounds containing magnetic M^{II} dications show supertransferred hyperfine fields at the antimony, the magnitudes of which may be related to the nature and distribution of the dications.

Introduction

The spinel antimonates of stoichiometry $M^{II}_4M^{III}Sb^{V}O_8$ and $M^{II}_5M^{III}_3Sb^{V}O_{12}$, in which M^{II} is a divalent and M^{III} a trivalent transition-metal cation, have been synthesized[1] and studied by X-ray diffraction, infrared, and Mössbauer spectroscopy.[2,3] In order to simplify the comparison between spinels of different stoichiometry we will use the triple and double formulas

$$[M^{II}_4M^{III}Sb^{V}O_8]_3 = M^{II}_{12}M^{III}_3Sb^{V}_3O_{24}$$

$$[M^{II}_5M^{III}_3Sb^{V}O_{12}]_2 = M^{II}_{10}M^{III}_6Sb^{V}_2O_{24}$$

presented in Table I. The X-ray results reveal two different crystallographic structures in these spinels. The first structure is face-centered cubic and is represented in this paper by $Zn_{12}Fe_3Sb_3O_{24}$ and $Ni_{10}Fe_6Sb_2O_{24}$ with $Fd3m$ (O_h^7-No. 227) space group.[1,3] The second structure is orthorhombic[1] with the most likely space group $Imma$ (D_{2h}^{28}-No. 74) and is represented in this paper by the additional compounds listed in Table I. From a combined X-ray, infrared, and Mössbauer spectral study, it has been proposed[1,2] that the M^{III} cations are present on the tetrahedral (A, 4e) and octahedral (B, 4c) sites in the ratio of two to one. Further, a two to one order on each geometric site was proposed such that the occupancy of the tetrahedral 8h site was twice that of the 4e site and the combined occupancy of the octahedral 8g and 8h sites was twice that of the 4c and 4b sites. This leads to the general formula $((8h)_4(4e)_2)[(8h, 8g)_8(4c)_2(4b)_2]O_{24}$, where only antimony is found on the octahedral 4b site.

In this paper we report iron-57 Mössbauer-effect spectra obtained below the magnetic ordering temperature. This work, which completes the preliminary results presented earlier,[2] also permits a more accurate analysis of the paramagnetic spectra and leads to a revision of the various cation distributions presented earlier.[1] In addition, we report the antimony-121 Mössbauer-effect spectra, certain of which show a supertransferred hyperfine field at the antimony nucleus. These results are discussed and compared with other studies of the transferred hyperfine fields in antimony-121, tin-119, and tellurium-125 spinels.

Experimental Section

The iron-57 Mössbauer-effect spectra were obtained on either a Ranger Scientific or a Harwell constant-acceleration spectrometer both of which used a room-temperature rhodium matrix source and were calibrated at room temperature with natural α-iron foil. Spectra obtained at 4.2 K and below used a cryostat in which the sample was placed directly in liquid helium. The sample temperature was measured by determining the vapor pressure above the liquid helium. Least-squares minimization programs implemented on the IBM 370/168 at Harwell and Amdahl 7 at the University of Missouri were used to analyze the iron-57 spectra. This analysis indicates that the isomer shift and quadrupole shift values reported below are accurate to at least ±0.02 mm/s. The hyperfine fields are accurate to at least ±1 kOe and in some instances to ca. ±0.5 kOe. The error in Γ and $\Delta\Gamma$ is ca. ±0.02 mm/s except in those compounds with large values of Γ and $\Delta\Gamma$ in which case their error limits may be substantially higher. The 4.2 K antimony-121 spectra were obtained with a vertical-configuration Harwell spectrometer with both the source and absorber placed directly in liquid helium. For the room-temperature studies both the source and absorber were at room temperature. The spectrometer was calibrated at room temperature with natural α-iron foil and at 4.2 K and InSb, and the isomer shifts are reported relative to $CaSnO_3$. The antimony spectra were fit to a combined magnetic and quadrupole interaction under the assumption of an axially symmetric field gradient pointing along the magnetic field direction. The values for the ground-state moment, the ratio of moments, and the ratio of quadrupole moments were taken from ref 4, and the intensities of the hyperfine components were those given in Greenwood and Gibb.[5] The parameters varied in the fit were the isomer shift and the internal hyperfine field or the quadrupole interaction. Either two or three sites were assumed. The quadrupole parameter from the fit is $1/4e^2qQ$, where Q refers to the ground-state quadrupole moment. The line width

* To whom correspondence should be addressed at the University of Missouri—Rolla.

(1) Tarte, P.; Preudhomme, J. *J. Solid State Chem.* **1979**, *29*, 273.
(2) Gérard, A.; Grandjean, F.; Preudhomme, J.; Tarte, P. *J. Phys., Colloq. (Orsay, Fr.)* **1979**, *49*, C2-339.
(3) Preudhomme, J.; Tarte, P.; Kenens, R.; Grandjean, F.; Gérard, A. *Bull. Cl. Sci. Acad. R. Belg.* **1980**, *66*, 776.
(4) Stevens, J. G.; Stevens, V. E. "Mössbauer Effect Data Index, Covering the 1976 Literature"; Plenum Press: New York, 1978; p 122.
(5) Greenwood, N. N.; Gibb, T. C. "Mössbauer Spectroscopy"; Chapman and Hall: London 1971; pp 447, 258–268.

0020-1669/84/1323-1886$01.50/0

Table I. Stoichiometry, Cation Distribution, Ordering Temperature, and Paramagnetic Mössbauer-Effect Spectral Data[a]

compd	cation distribn $(A, T_d)_8[B, O_h]_{12}O_{24}$	T_t, K	T, K	tetrahedral A site				octahedral B site				impurity			
				δ	ΔE_Q	Γ	% A	δ	ΔE_Q	Γ	% A	δ	ΔE_Q	Γ	% A	χ^2
$Zn_{12}Fe_3Sb_3O_{24}$ [b]	$(Zn_6)[Zn_6Fe_3Sb_3]O_{24}$	~1.35	296	[c]				0.34	0.53	0.33	100	[c]				1.33
			78	[c]				0.44	0.55	0.36	100	[c]				1.17
			4.2	[c]				0.44	0.54	0.41	100	[c]				1.07
			1.12	[c]				0.38	0.63	0.97	7	[c]				1.43
$Mg_{12}Fe_3Sb_3O_{24}$ [d]	$(Mg_4Fe_2)[Mg_6FeSb_3]O_{24}$	~5	296	0.22	1.10	0.41	53.2	0.25	0.50	0.40	46.8	[c]				3.20
			78	0.32	1.12	0.42	54.6	0.44	0.52	0.42	45.4	[c]				2.12
			4.2	0.45	0.91	0.61	5.2									1.14
$Co_{12}Fe_3Sb_3O_{24}$ [d]	$(Co_4Fe_2)[Co_8FeSb_3]O_{24}$	210	296	0.26	0.92	0.37	62.5	0.37	0.38	0.31	32.8	0.22	0.45	0.21	4.7	1.52
$Co_3Ni_9Fe_3Sb_3O_{24}$ [d]	$(Co_3Ni_{0.67}Fe_{2.33})[Ni_{8.33}Fe_{0.67}Sb_3]O_{24}$	230	295	0.26	1.06	0.36	74.2	0.36	0.40	0.24	21.5	0.22	0.30	0.24	4.3	0.84
$Mg_3Ni_9Fe_3Sb_3O_{24}$ [d]	$(Mg_3Ni_{0.70}Fe_{2.30})[Ni_{8.30}Fe_{0.70}Sb_3]O_{24}$	175	296	0.25	1.10	0.40	71.8	0.38	0.41	0.27	21.8	0.26	0.39	0.31	6.5	1.12
$Mg_6Ni_6Fe_3Sb_3O_{24}$ [d]	$(Mg_{3.80}Fe_{2.20})[Ni_6Mg_{2.20}Fe_{0.80}Sb_3]O_{24}$	190	295	0.24	1.09	0.39	70.6	0.34	0.40	0.29	25.9	0.43	0.40	0.19	3.5	1.61
$Ni_{10}Fe_6Sb_2O_{24}$ [b]	$(Ni_{1.17}Fe_{4.83})[Ni_{8.83}Fe_{1.17}Sb_2]O_{24}$	>590														

[a] All data in mm/s, δ relative to room-temperature natural α-iron foil. [b] Cubic. [c] Component not observed. [d] Orthorhombic. In these compounds, the first four tetrahedral cations occupy the 8h site, the second two the 4c site. The first eight octahedral cations occupy the 8g and 8h sites, the last four the 4c and 4b sites with only antimony on the 4b site. The general formula is $((8h)_4(4e)_2)$-$[(8h,8g)_6(4c)_2(4b)_2]O_{24}$.

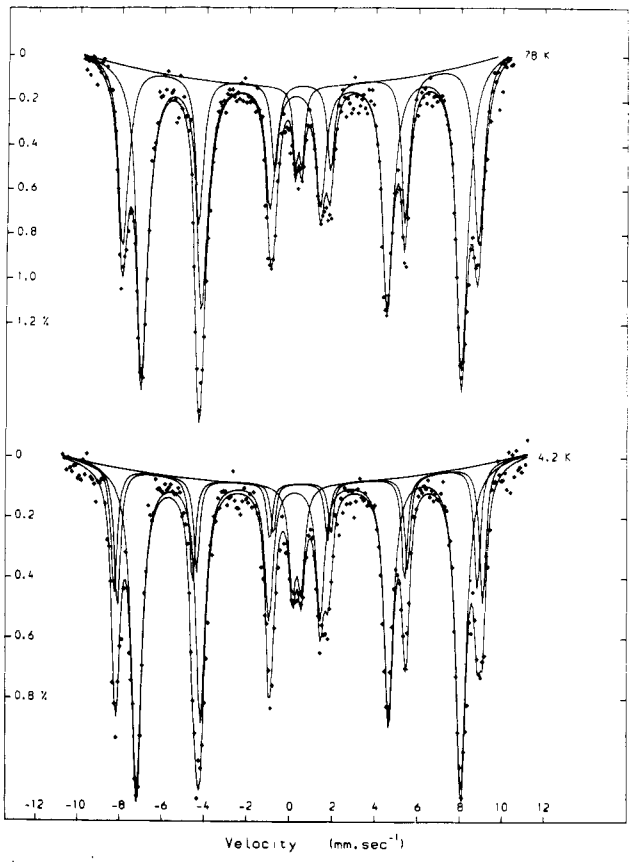

Figure 1. Iron-57 Mössbauer-effect spectra of $Co_{12}Fe_3Sb_3O_{24}$ obtained at 78 and 4.2 K. The solid lines are the result of a least-squares fit described in the text.

was fixed at 2.47 mm/s for all fits. The errors associated with the fits obtained were estimated by assuming that each data point is the mean of a normal distribution whose standard deviation is the square root of the data point. For each data point, a random number is generated from this normal distribution to represent a new point (as if the spectrum had been remeasured). The resulting "new" spectrum is fitted in the normal way to give a new set of parameters. By using 20 such randomly generated spectra, it is possible to calculate the standard deviation of the resulting spectral fitting parameters. This error, which is in fact overestimated because of increased statistical fluctuations, is taken as the error in the actual determination and is presented for selected compounds in Table IV.

The samples are the same as those studied previously, and the preparation of the materials is described in ref 1 and 3.

Results and Discussion

Magnetically Ordered Iron-57 Mössbauer-Effect Spectra. Preliminary Mössbauer-effect spectra were used[2,3] to determine the magnetic ordering temperature for the spinels under study, and the resulting transition temperatures are reported in Table I. In this study each of the samples has been measured at 78 and 4.2 K and at 1.12 K if there was no indication of magnetic ordering at 4.2 K. The results obtained at 78 and 4.2 K for the ordered compounds are shown in Figure 1 for $Co_{12}Fe_3Sb_3O_{24}$, in Figure 2 for $Co_3Ni_9Fe_3Sb_3O_{24}$, in Figure 3 for $Mg_3Ni_9Fe_3Sb_3O_{24}$, and in Figure 4 for $Ni_{10}Fe_6Sb_2O_{24}$. It is clear that each spectrum displays a small paramagnetic impurity, the nature of which is discussed below. The magnetic spectra were fit by superimposing two or three magnetic sextets. The adjustable parameters were the internal hyperfine field, H_{int}, the quadrupole shift, QS, the isomer shift, δ, and the line width, Γ. The relative area of each line in a sextet was held fixed at 3/2/1/1/2/3, but the relative area of each sextet was in general unconstrained. The line width of the inner lines, Γ, was increased by $0.5\Delta\Gamma$ and $\Delta\Gamma$ for the two–five and one–six lines, respectively. The most reasonable value of

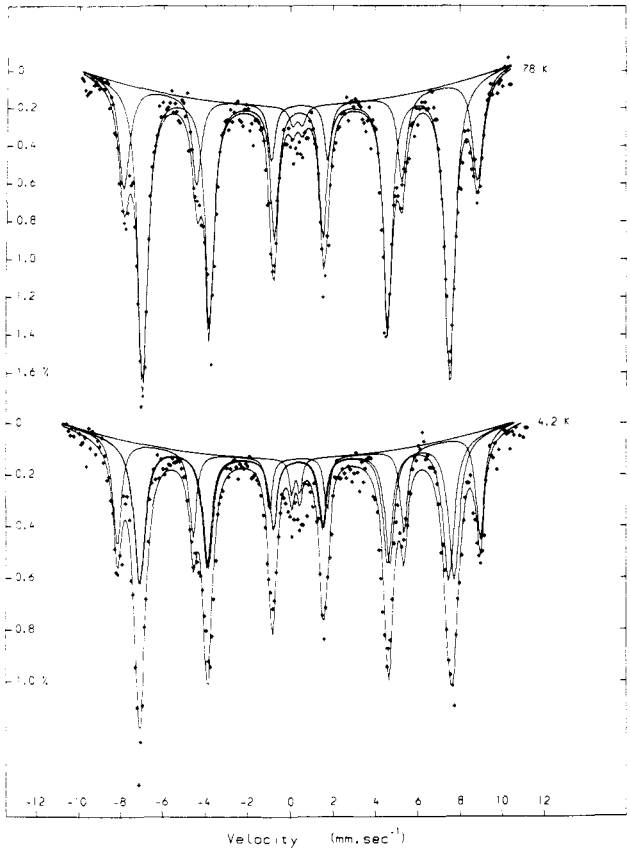

Figure 2. Iron-57 Mössbauer-effect spectra of $Co_3Ni_9Fe_3Sb_3O_{24}$ obtained at 78 and 4.2 K. The solid lines are the result of a least-squares fit described in the text.

$\Delta\Gamma$ was obtained from preliminary fits and was constrained in the final fits. The final fits are illustrated by the solid lines in Figures 1–4 and yield the various hyperfine parameters presented in Table II.

In the evaluation of the Mössbauer-effect spectra of spinels it is often assumed[5] that the relative area of absorption of the tetrahedral A site and the octahedral B site is proportional to the relative iron population on each of the sites; i.e., the recoil-free fractions for the two sites are the same. If we make this assumption, it is possible to determine the A/B iron occupancy ratio and the stoichiometry of the compound. We have determined the average A/B iron occupancy ratio for each compound from its magnetic spectrum. In addition, we have determined the approximate range of A/B values that are consistent with the magnetic spectra. This range of values, which is reported in detail in Table III (see supplementary material) was determined by constraining the hyperfine parameters to the values given in Table II and allowing the least-squares minimization computer program to evaluate the A/B iron occupancy ratio from an initially very high and very low input ratio. The results of this evaluation seem internally consistent and indicate, with the exception of $Co_3Ni_9Fe_3Sb_3O_{24}$, that the apparent A/B iron occupancy ratio decreases with decreasing temperature. Because the assumption of equivalent recoil-free fractions for the two sites is most reasonable at the lowest temperatures, we have used the ratio obtained at 4.2 K to calculate the optimum cation distribution given in Table I. In these formulas, the fractional stoichiometric occupancies are valid to at least ±0.02 as illustrated in Table III. At 78 K, the substantial apparent increase in the A/B iron occupancy ratio for three of the compounds seems to indicate, at least for these compounds, that the recoil-free fraction for the tetrahedral A site is larger than that of the octahedral B site, because of the different temperature dependences of the recoil-free fractions. The different temperature dependence of

Table II. Mössbauer-Effect Spectral Data–Ordered Phase[a]

		tetrahedral A site					octahedral B site					impurity				A/B iron site area ratio	χ^2
compd	T, K	δ	QS	H_{int}	Γ	$\Delta\Gamma$	% A	δ	QS	H_{int}	Γ	$\Delta\Gamma$	% A	δ	ΔE_Q	Γ	% A		
$Zn_{12}Fe_3Sb_3O_{24}$	1.12							0.46	0.08	436	0.87	1.06	93[c]	*b*				0	1.43
$Mg_{12}Fe_3Sb_3O_{24}$	4.2	0.37	−0.05	210	1.83	3.06	63.2	0.41	−0.11	356	1.33	0.58	31.6[c]	*b*				2.0	1.53
	1.12	0.43	−0.07	377	0.89	0.42	66.7	0.45	−0.11	423	0.74	0.37	33.3	*b*				2.0	2.28
$Co_{12}Fe_3Sb_3O_{24}$	78	0.36	−0.18	466	0.53	0.11	63.8	0.48	0.03	519	0.39	0.19	32.2	0.30	0.30	0.43	3.9	2.0 (1)	1.30
	4.2	0.36	−0.10	472	0.49	0.12	62.1	0.47	−0.04	533	0.32	0.07	15.5	0.35	0.41	0.51	7.0	2.00 (6)	1.25
								0.45	0.14	529	0.32	0.07	15.5						
$Co_3Ni_9Fe_3Sb_3O_{24}$	78	0.35	0.05	448	0.40	0.20	71.9	0.47	−0.03	516	0.34	0.24	25.4	0.35	0.37	0.33	2.7	2.83 (1)	1.42
	4.2	0.31	0.08	448	0.41	0.21	37.1	0.43	−0.01	529	0.32	0.14	21.5	0.32	0.42	0.35	4.3	3.45 (5)	1.63
		0.37	0.03	457	0.41	0.21	37.1												
$Mg_3Ni_9Fe_3Sb_3O_{24}$	78	0.32	0.26	425	0.42	0.21	37.3	0.46	−0.03	497	0.37	0.17	19.7	0.27	0.35	0.60	5.6	3.80 (4)	0.72
		0.34	−0.03	436	0.42	0.21	37.3												
	4.2	0.33	0.25	447	0.44	0.05	35.9	0.44	0.01	533	0.34	0.05	21.8	0.37	0.41	0.60	6.5	3.30 (9)	0.83
		0.37	−0.20	457	0.44	0.05	35.9												
$Mg_6Ni_6Fe_3Sb_3O_{24}$	78	0.30	−0.01	404	0.68	0.10	37.8	0.44	−0.05	481	0.41	0.10	21.2	0.27	0.09	0.65	3.6	3.58 (3)	1.08
		0.35	−0.05	428	0.55	0.10	37.8												
	4.2	0.32	−0.03	446	0.61	0.14	70.6	0.43	−0.02	523	0.41	0.06	25.9	0.29	0.41	0.74	3.5	2.73 (5)	1.51
$Ni_{10}Fe_6Sb_2O_{24}$	78	0.35	−0.02	471	0.51	0.19	83.4	0.45	−0.01										
	4.2	0.35	0.01	472	0.52	0.20	77.9	0.44	0.02	544	0.24	0.10	15.0	0.31	0.32	0.38	1.6	5.56 (10)	1.68
										547	0.33	0.09	18.9	0.32	0.49	0.45	3.2	4.11 (9)	1.84

[a] All data except H_{int} in mm/s, δ relative to room-temperature natural α-iron foil, H_{int} given in kOe. [b] Component not observed. [c] The paramagnetic component parameters are given in Table I.

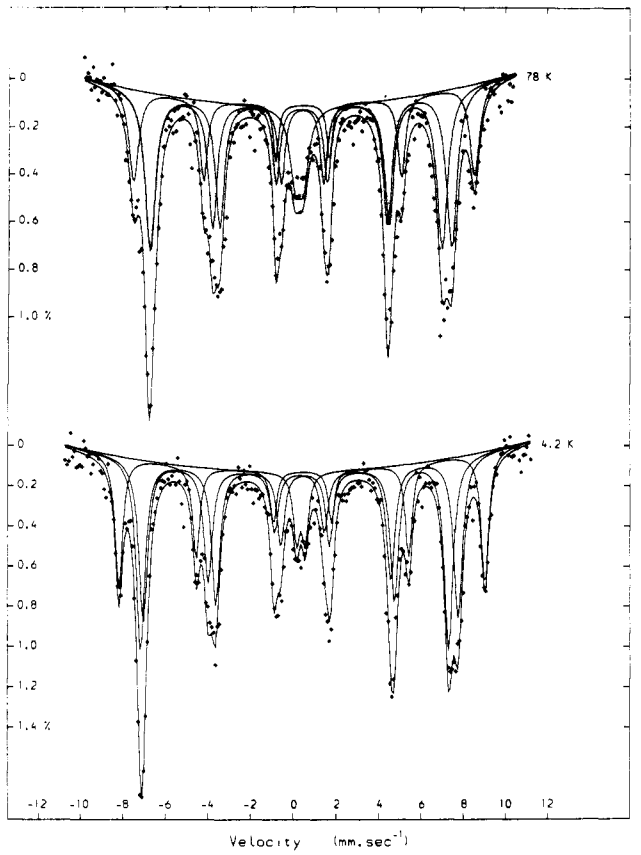

Fig. 3. Iron-57 Mössbauer-effect spectra of $Mg_3Ni_9Fe_3Sb_3O_{24}$ obtained at 78 and 4.2 K. The solid lines are the result of a least-squares fit described in the text.

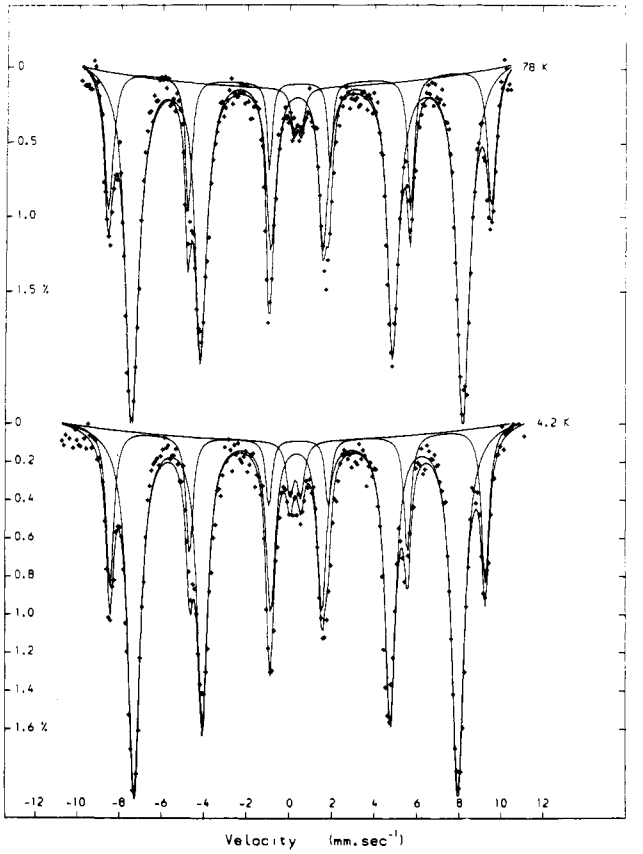

Figure 4. Iron-57 Mössbauer-effect spectra of $Ni_{10}Fe_6Sb_2O_{24}$ obtained at 78 and 4.2 K. The solid lines are the result of a least-squares fit described in the text.

the A/B iron occupancy ratio for $Co_3Ni_9Fe_3Sb_3O_{24}$ is difficult to understand but may be related to the different numbers of magnetic sextets used in the different fits. It is interesting that A/B in $Co_{12}Fe_3Sb_3O_{24}$ is essentially independent of temperature.

The room-temperature Mössbauer spectrum of $Co_{12}Fe_3Sb_3O_{24}$ agrees well with earlier work,[2] and the 78 K spectrum (see Figure 1) is well fit by two magnetic sextets plus an impurity doublet. The relative areas of the magnetic sextets confirm the cation distribution observed in the room-temperature spectrum. At 4.2 K the Mössbauer spectral lines at 5.5 and 9 mm/s are broadened, and at this temperature two magnetic sextets are required to fit the octahedral B site contribution as is shown in Figure 1. These two sites differ in their quadrupole shifts and hyperfine fields (ΔH_{int} = 4 (1) kOe) and have the same intensities. The existence of differing hyperfine fields on the B sites has been reported earlier[6] and attributed to a statistical occupation of the A sites by different cations. The different cations perturb the strong A–B ferromagnetic exchange pathways and can result in B-site iron(III) hyperfine fields that differ by as much as 10–20 kOe. In $(Co_4Fe_2)[Co_8FeSb_3]O_{24}$ the B-site iron(III) ions (which occupy the 4c position[1] in space group *Imma*) have four cobalt(II) and two iron(III) neighbors on the A sites. It is not in this case possible to distinguish different environments for the iron(III) ions on the A sites. Actually the hyperfine field difference mainly reflects a narrow distribution of hyperfine fields, which could be due to the random distribution of antimony(V) and iron(III) on the 4c octahedral B site and would also account for the different quadrupole shifts. Because the antiferromagnetic B–B interactions are weak, the presence of antimony(V) as the nearest neighbor of iron(III) has only a very slight influence upon the hyperfine field at the iron(III).

The situation is different for the magnetic components in the Mössbauer spectra of the nickel-containing antimony spinels. For these compounds the octahedral B site could always be fit with a single sextet representing, at most, a very small distribution of fields. However, in several instances, the tetrahedral A site requires two magnetic sextets to fit the observed intensity pattern. The presence of the two A-site hyperfine fields is clearly shown in Figures 2 and 3. The one exception to this is $Ni_{10}Fe_6Sb_2O_{24}$, which, as shown in Figure 4, may be fit with one sextet for each site with the A/B iron occupancy ratio of 4.11 (9). This area ratio leads to the cation distribution shown in Table I and is consistent with the suggestion of Blasse[7] that 20% of the nickel(II) ions are present on the tetrahedral A site. This distribution is also in good agreement with the known preference of the nickel for the octahedral site, which results in the displacement of some of the iron(III) from the octahedral B sites to the tetrahedral A sites. This of course disturbs the 2:1 iron occupancy ratio between the A and B sites that was observed in $Co_{12}Fe_3Sb_3O_{24}$.

The low-temperature Mössbauer spectra of $Co_3Ni_9Fe_3Sb_3O_{24}$ are illustrated in Figure 2 and reveal distinct broadening of the lines at 4.5 and 8 mm/s at 4.2 K, which justifies the introduction of two magnetic sextets on the tetrahedral A site. For $Mg_3Ni_9Fe_3Sb_3O_{24}$ (see Figure 3) a similar broadening justifies the introduction of the two sextets both at 78 and at 4.2 K. In each instance the two sextets attributed to the A site differ principally in their hyperfine fields.

The cation distributions given in Table I indicate the strong preference of nickel(II) for the octahedral B sites and the site indifference of cobalt(II) and magnesium(II). These distributions are different from those proposed previously[1] because

(6) Ok, H. N.; Evans, B. J. *Phys. Rev. B.: Solid State* **1976**, *14*, 2956.

(7) Blasse, G. Doctoral Thesis, Eindhoven University, The Netherlands, 1964.

the presence of the impurity was not considered in fitting the paramagnetic spectra. Because in the distributions $(Co_3Ni_{0.67}Fe_{2.33})[Ni_{8.33}Fe_{0.67}Sb_3]O_{24}$, $(Mg_3Ni_{0.70}Fe_{2.30})[Ni_{8.30}Fe_{0.70}Sb_3]O_{24}$, and $(Mg_{3.80}Fe_{2.20})[Ni_6Mg_{2.20}Fe_{0.80}Sb_3]O_{24}$ there are more than two iron(III) ions on the A sites, they must occupy both available tetrahedral positions 8h and 4e of the orthorhomibc structure[1] and share these sites with nickel(II), cobalt(II), or magnesium(II) ions. The tetrahedral 4e site has 12 first neighbors on the octahedral B sites (2 × 4c, 8 × 8h, 2 × 8g) that are mainly occupied by nickel(II) ions in $(Co_3Ni_{0.67}Fe_{2.33})[Ni_{8.33}Fe_{0.67}Sb_3]O_{24}$ and $(Mg_3Ni_{0.70}Fe_{2.30})[Ni_{8.30}Fe_{0.70}Sb_3]O_{24}$ and by nickel(II), iron(III), and magnesium(II) in $(Mg_{3.80}Fe_{2.20})[Ni_6Mg_{2.20}Fe_{0.80}Sb_3]O_{24}$. In contrast, the tetrahedral 8h site has 12 octahedral B-site first neighbors (6 × 8g, 3 × 8h, 3 × 4b); i.e., it has antimony(V), nickel(II), or magnesium(II) and iron(III) ions as first neighbors on this site. Thus, it is not surprising that the tetrahedral 4e and 8h sites differ somehwat in their internal hyperfine fields. If these distributions are correct, then the 2/1 order on both the tetrahedral and octahedral sites is not preserved because of the mixing of the ions on both sites. The resulting structure may not conform to that expected for the thermodynamic ground state that would be obtained from truly reversible cooling from the melt, but the results seem reasonable for the actual cooling procedures used.

It is perhaps surprising that no splitting of the octahedral B-site magnetic sextet in the nickel antimony spinels is observed as is the case in $Co_{12}Fe_3Sb_3O_{24}$ (see Figure 1). However, in the nickel spinels the line widths of the B site are smaller than those on the A site and a second internal hyperfine field is not needed. In $Ni_{10}Fe_6Sb_2O_{24}$, no splitting of either of the magnetic sextets is observed, most likely because in this compound, which has a magnetic ordering temperature above 590 K, the magnetic hyperfine fields on each site are fully saturated to essentially the same value. Nevertheless, the 0.5 mm/s line width observed for the tetrahedral A site indicates a small distribution of hyperfine fields. The cation distributions in $(Co_3Ni_{0.67}Fe_{2.33})[Ni_{8.33}Fe_{0.67}Sb_3]O_{24}$ and $(Mg_3Ni_{0.70}Fe_{2.30})[Ni_{8.30}Fe_{0.70}Sb_3]O_{24}$ differ only slightly in their A-site occupancy. Therefore their A-site saturation hyperfine fields should be very similar, as is observed at 4.2 K in Table II. The fields differ more at 78 K because the two compounds have magnetic ordering temperatures that differ by 55 K.

Several general conclusions may be drawn from the magnetic spectra shown in Figures 1–4. First, the isomer shift difference between the octahedral B site and the tetrahedral A site is approximately constant at 0.1–0.2 mm/s as is usually observed for spinels.[5] As expected, the higher coordination number of the octahedral B site leads to the higher isomer shift. Second, the tetrahedral A-site hyperfine fields are smaller than the B-site fields. Third, the quadrupole shifts, which are a function of the quadrupole interaction, the asymmetry parameter, and the Euler angles relating the EFG tensor to the hyperfine field direction, are not easily interpreted. They are, however, small as would be expected of the approximately cubic geometry of both the tetrahedral and octahedral sites. Finally, it is interesting to compare the saturation hyperfine fields of the different compounds. Both $Co_{12}Fe_3Sb_3O_{24}$ and $Co_3Ni_9Fe_3Sb_3O_{24}$, which have similar A-site occupancies, show very similar hyperfine fields on the B site. $Mg_6Ni_6Fe_3Sb_3O_{24}$, which has no nickel(II) and hence a minimum of unpaired electron spin on the A site, has the lowest saturation field on the B site (see Table II), whereas $Ni_{10}Fe_6Sb_2O_{24}$, which has the largest number of unpaired electron spins on the A site, has the highest saturation field on the B site. On this basis, it is then surprising that $Mg_3Ni_9Fe_3Sb_3O_{24}$ and $Co_3Ni_9Fe_3Sb_3O_{24}$ show quite similar internal fields on the B site, indeed among the A-site neighbors of iron on the 4c site, three

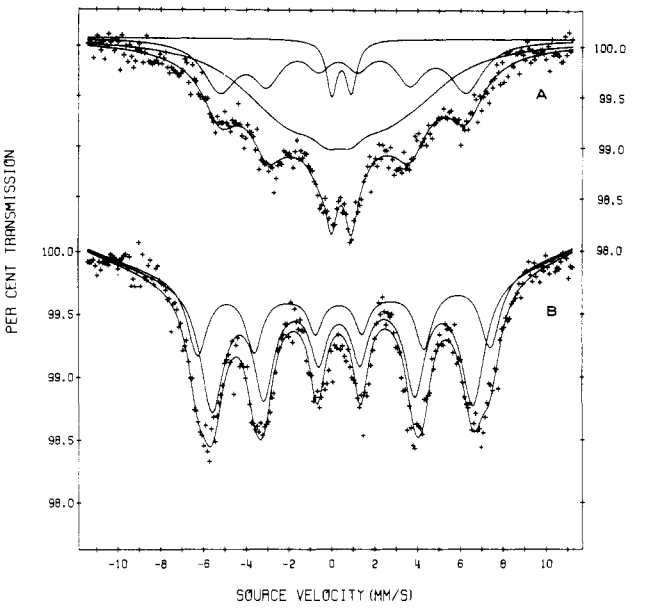

Figure 5. Iron-57 Mössbauer-effect spectra of $Mg_{12}Fe_3Sb_3O_{24}$ obtained at 4.2 and 1.12 K. The solid lines are the result of a least-squares fit described in the text.

magnesium(II) ions are replaced by three cobalt(II) ions (see Table IV).

The spectra of orthorhombic $Mg_{12}Fe_3Sb_3O_{24}$ at 1.12 and 4.2 K are shown in Figure 5. The 1.12 K fit results from the superposition of two magnetic sextets, the parameters of which are given in Table II. In this fit, and the fit at 4.2 K, the A/B iron occupancy ratio for the magnetic sextets has been constrained to 2.0. At 4.2 K this compound gives a complex spectrum apparently composed of an octahedral B-site magnetic sextet that is fairly well resolved with an internal hyperfine field of ca. 350 kOe, a poorly resolved magnetic sextet with a field of ca. 210 kOe, and a paramagnetic doublet with the hyperfine parameters given in Table I. The latter two components are associated with the partially ordered tetrahedral A site. As expected, the line widths for these magnetic components are very high as indicated in Table II. Hence, the ordering temperature of $Mg_{12}Fe_3Sb_3O_{24}$ is apparently somewhat above 4.2 K. The cubic $Zn_{12}Fe_3Sb_3O_{24}$ compound, which contains only iron(III) on the B site, is not ordered at 4.2 K but is ordered at 1.35 K, and the spectrum obtained at 1.12 K is illustrated in Figure 6. At 1.12 K the spectrum is fit with a doublet and a magnetic sextet whose parameters are given in Tables I and II. In this case the doublet may be attributed to some of the B-site iron(III) that is not ordered at 1.12 K. In a similar instance in the spinel $Fe_{2-2y}Mg_{1+y}Ti_yO_4$, with $y \geq 0.4$, it was found[8] that *some* of the iron(III) ions did not participate in the ferromagnetism observed in these materials. This behavior was explained on the assumption that each iron(III) ion must have at least two superexchange pathways of the type Fe_A^{3+}–O^{2-}–Fe_B^{3+} in order to couple the iron(III) magnetic moment to its neighbors at all temperatures below the transition temperature. A similar type of argument accounts for the low ordering temperature in both $Zn_{12}Fe_3Sb_3O_{24}$ and $Mg_{12}Fe_3Sb_3O_{24}$, the very different values for the magnetization at each type of site in $Mg_{12}Fe_3Sb_3O_{24}$, and the observation of a paramagnetic component in $Zn_{12}Fe_3Sb_3O_{24}$ even at 1.12 K. The large line width of the magnetic sextet indicates a field distribution due either to different unresolved hyperfine fields or to sample imperfections similar to those found in $ZnFe_2O_4$.[9] Both the ordering temperature and hy-

(8) De Grave, E.; Dauwe, C.; Govaert, A.; De Sitter, J. *Appl. Phys.* **1977**, *12*, 131.
(9) Varret, F.; Gérard, A.; Imbert, P. *Phys. Status Solidi B* **1971**, 723.

Table IV. Antimony-121 Mössbauer-Effect Spectral Parameters and Supertransferred Hyperfine Fields[a]

compd	300 K					4.2 K							
	δ	$^1/_4e^2qQ$	H_{int}	% A	χ^2	δ	$^1/_4e^2qQ$	H_{int}	% A	χ^2	assgnt	Sb occup	T_d A-site near neighbors	$H^{calcd}_{int,Sb}$
$Zn_{12}Fe_3Sb_3O_{24}$	−0.52	3.29	b	100	0.9	−0.42	5.36	b	100	1.1	16c	2	6 Zn(II)	0
$Mg_{12}Fe_3Sb_3O_{24}$	−0.07	5.43	b	100	1.0	−0.05	6.84	b	100	1.4	4c, 4b	1, 2	6 Mg(II)	0
$Co_{12}Fe_3Sb_3O_{24}$						−0.77	b	263	9	1.2	4c	1	4 Co(II), 2 Fe(III)	270
						−0.79	b	203	34					
						−0.84	b	143	57		4b	2	6 Co(II)	234
$Co_9Ni_3Fe_3Sb_3O_{24}$	−0.90	6.00	b	100	1.0	−0.77	b	287	5	1.1	4c	1	3 Co(II), 0.67 Ni(II), 2.33 Fe(III)	262
						−0.79	b	195	36					
						−0.84	b	140	59		4b	2	4.5 Co(II), 1.0 Ni(II), 0.5 Fe(III)	222
$Mg_3Ni_9Fe_3Sb_3O_{24}$	−0.64	4.66	b	100	2.0	−0.60	b	139	60	1.0	4c	1	3 Mg(II), 0.7 Ni(II), 2.3 Fe(III)	144
						−0.60	b	53	40		4b	2	4.5 Mg(II), 1.0 Ni(II), 0.5 Fe(III)	47
$Mg_6Ni_6Fe_3Sb_3O_{24}$	−0.45 (2)	4.23 (27)	b	100	1.1	−0.51	b	126	57	1.1	4c	1	4 Mg(II), 2 Fe(III)	114
						−0.36	b	38	43		4b	2	6 Mg(II)	0
$Ni_{10}Fe_6Sb_2O_{24}$	−0.79	b	261	16[d]	0.9	−0.7 (2)	b	263 (12)	16 (4)	0.8				
	−0.92	b	177	45		−0.79 (4)	b	193 (6)	45 (6)		16c	2	1.2 Ni(II), 4.8 Fe(III)	296
	−0.95	b	117	39		−0.84 (5)	b	143 (4)	39 (6)					

[a] All data in mm/s, δ relative to $CaSnO_3$ at either 300 or 4.2 K, H_{int} given in kOe, all Γ fixed at 2.47 mm/s. [b] Value constrained to zero. [c] The octahedral antimony 4c site has four 8h and two 4e tetrahedral A-site near neighbors, whereas the antimony 4b site has six 8h tetrahedral A-site near neighbors. [d] These percent areas were constrained to the values obtained at 4.2 K.

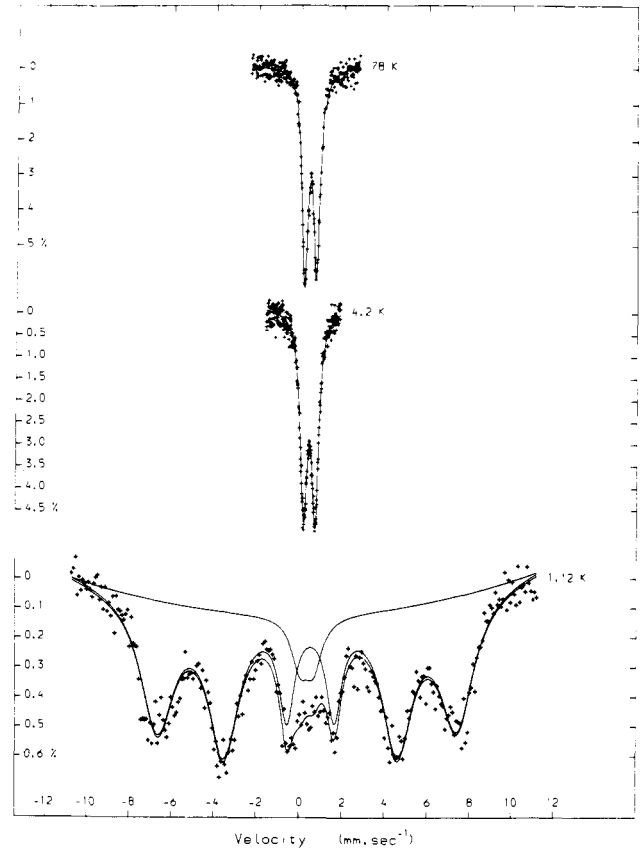

Figure 6. Iron-57 Mössbauer-effect spectra of $Zn_{12}Fe_3Sb_3O_{24}$ obtained at 78, 4.2, and 1.12 K. The solid lines are the result of a least-squares fit described in the text.

perfine field are lower than found in $ZnFe_2O_4$ as would be expected because the B sites are occupied by iron(III), zinc(II), and antimony(V) in $Zn_{12}Fe_3Sb_3O_{24}$ and only by iron(III) in $ZnFe_2O_4$.

Paramagnetic Impurity. Although it is not apparent from the room-temperature spectra, the lower temperature magnetic spectra reveal the presence of a small nonmagnetic impurity present to the extent of a few percent. Because the amount of the impurity is best determined in the ordered spectra, we have refit the room-temperature paramagnetic spectra by constraining the relative area of each component to that observed at low temperature. The results are presented in Table I and reveal parameters for the A and B sites that are very similar to those reported earlier.[2] On the basis of the impurity Mössbauer parameters given in Table II, the impurity appears to be the same in each case. The impurity isomer shift seems characteristic of iron(III) in a tetrahedral oxide site whereas the quadrupole interaction is more typical of an iron(III) in an octahedral oxide site.

Several different possibilities exist for the nature of this impurity, which is not detected in the X-ray powder diffraction patterns for the materials. First, it could be an unidentified compound with an ordering temperature below 4.2 K. On the basis of the quadrupole interaction, both $FeSbO_4$[10] and $Mg_2Fe_2Sb_2O_6$[11] may be excluded. Second, it could be a superparamagnetic phase of the compound or a superparamagnetic impurity. Because all samples have ordering temperatures above 175 K, it seems rather unlikely that some of the material would remain unordered at 4.2 K. Furthermore, the hyperfine parameters of the impurity are not similar to those found in the paramagnetic state, which seems to elim-

(10) Wooten, J. B.; Long, G. G.; Bowen, L. H. *J. Inorg. Nucl. Chem.* **1974**, *36*, 2177.
(11) Grandjean, F., unpublished results.

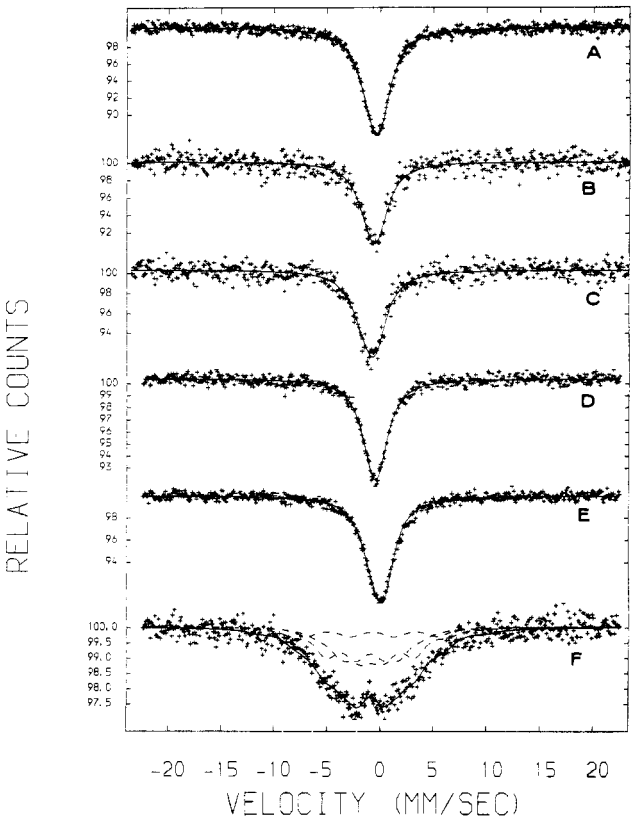

Figure 7. Antimony-121 Mössbauer-effect spectra of $Mg_6Ni_6Fe_3Sb_3O_{24}$ (A), $Mg_3Ni_9Fe_3Sb_3O_{24}$ (B), $Co_3Ni_9Fe_3Sb_3O_{24}$ (C), $Zn_{12}Fe_3Sb_3O_{24}$ (D), $Mg_{12}Fe_3Sb_3O_{24}$ (E), and $Ni_{10}Fe_6Sb_2O_{24}$ (F) obtained at 300 K. The solid lines are the result of a least-squares fit described in the text.

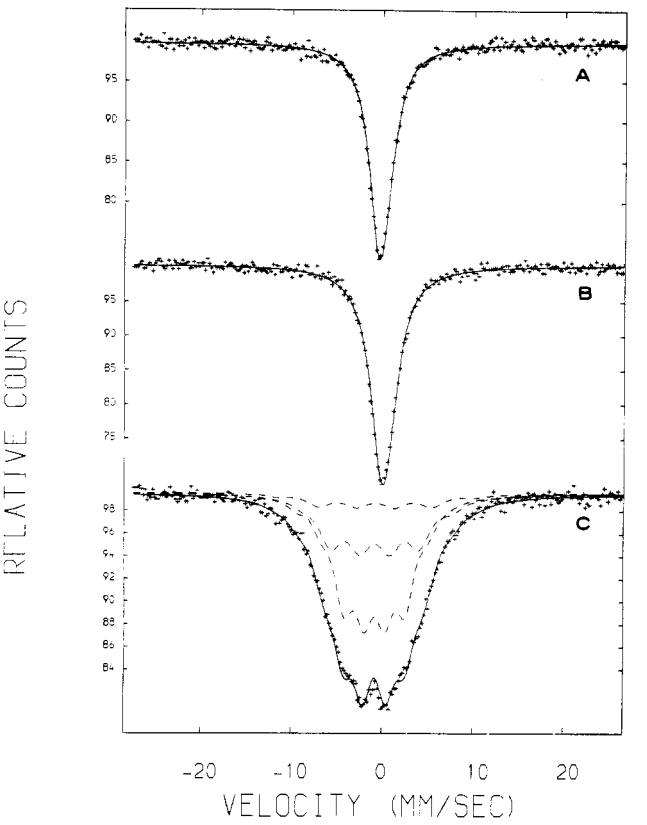

Figure 8. Antimony-121 Mössbauer-effect spectra of $Zn_{12}Fe_3Sb_3O_{24}$ (A), $Mg_{12}Fe_3Sb_3O_{24}$ (B), and $Co_{12}Fe_3Sb_3O_{24}$ (C) obtained at 4.2 K. The solid lines are the result of a least-squares fit described in the text.

inate the first possibility. Because there is little change in the area of the impurity between 78 and 4.2 K, we can exclude the second possibility. It seems certain that there would be a change in the amount of any superparamagnetic impurity that would be ordered between 78 and 4.2 K. Third, the impurity could be a magnetic compound that has been diluted in the spinel phase. In this case, the percentage of the material would have to be much larger than that indicated by the Mössbauer fraction, and one would then expect to see the material in the X-ray diffraction patterns, which is not the case. Finally, the impurity could be a glass, but the line widths of the impurity are not much larger than those of the magnetic components. Further, it seems unlikely that the slow quenching from high temperature used in the preparation[1] could result in the formation of a glass. At this time, all we can say about the impurity is that it contains iron(III), most likely in an oxide lattice, and remains paramagnetic down to 4.2 K. It may also contain antimony(V), but it would be difficult to detect it in the antimony-121 Mössbauer spectra (see below). The existence of this impurity does significantly modify the relative A- and B-site populations and has led to a revision (see Tables I and II) in the cation distribution proposed earlier for these materials.[2]

Evaluation of the Antimony-121 Mössbauer-Effect Spectra. The antimony-121 Mössbauer-effect spectra were measured with both the source and absorber at 4.2 K and, in some instances, with both the source and absorber at room temperature. The results are illustrated in Figures 7–9, and the resulting spectral parameters are presented in Table IV. All of the compounds studied at room temperature and $Zn_{12}Fe_3Sb_3O_{24}$ and $Mg_{12}Fe_3Sb_3O_{24}$ at 4.2 K show a single absorption envelope with at most a slightly resolved quadrupole interaction. The observed isomer shifts are characteristic of antimony(V) and confirm the so far assumed pentavalency of antimony. The quadrupole interactions observed at room temperature and in $Zn_{12}Fe_3Sb_3O_{24}$ and $Mg_{12}Fe_3Sb_3O_{24}$ at 4.2 K are of the same magnitude as the line widths and are in good agreement with the values of ca. 2.6 and 4.35 mm/s found respectively for the quadrupole interaction in $Zn_{14}Sb_4O_{24}$ and $Co_{14}Sb_4O_{24}$ by Evans.[12] Because $Zn_{12}Fe_3Sb_3O_{24}$ and $Mg_{12}Fe_3Sb_3O_{24}$ order magnetically at ca. 1.35 and 5 K, respectively, it is quite normal that no magnetic field is observed at the antimony in these compounds at 4.2 K as is easily seen in Figure 8.

All of the remaining compounds exhibit antimony-121 Mössbauer spectra that are considerably broadened at 4.2 K by the existence of a small supertransferred hyperfine field at the antimony nucleus. This supertransferred hyperfine field is clearly evident in Figures 8 and 9 and is not unexpected because all of these compounds have transition temperatures above 175 K (Table I). The hyperfine parameters for these spectra, as given in Table IV, are difficult to evaluate because of the large number of variable parameters associated with the overlapping subspectra. In order to simplify the fitting procedure, we have constrained each component to have a zero quadrupole interaction and the same line width. The variable parameters were then the isomer shift, hyperfine field, and relative area for each component, and the average line width. It was found that two different hyperfine fields were required to model the spectra of $Mg_3Ni_9Fe_3Sb_3O_{24}$ and $Mg_6Ni_6Fe_3Sb_3O_{24}$ whereas three fields were required for $Co_{12}Fe_3Sb_3O_{24}$, $Co_3Ni_9Fe_3Sb_3O_{24}$, and $Ni_{10}Fe_6Sb_2O_{24}$. Our results are very similar to those observed by Ruby et al.[13] and Evans[12] in the spinel series $Ni_{1+2x}Fe_{2-3x}Sb_xO_4$. Our $Ni_{10}Fe_6Sb_2O_{24}$ sample has the same stoichiometry as their sample with $x = 0.33$, and

(12) Evans, B. J. In "Mössbauer Effect Methodology" Gruverman, I. J., Ed.; Plenum Press: New York, 1966; Vol. 4, p 139.
(13) Ruby, S. L.; Evans, B. J.; Hafner, S. S. *Solid State Commun.* **1968**, *6*, 277.

Table V. Supertransferred Hyperfine Fields at Tin(IV), Antimony(V), and Tellurium(VI) in Spinel-Type Compounds[a]

compd	cation distribn	H_{int} on indicated ion, kOe			ref
$Fe_{17.7}Sn_{0.3}O_{24}$ (1)	$(Fe_6)[Fe^{2+}_{6.3}Fe_{5.4}Sn_{0.3}]O_{24}$		239		16
$Ni_{6.75}Fe_{10.5}Sn_{0.75}O_{24}$ (2)	$(Fe_6)[Ni_{6.75}Fe_{4.5}Sn_{0.75}]O_{24}$		250		16
$Co_{6.3}Fe_{11.4}Sn_{0.3}O_{24}$ (3)	$(Fe_6)[Co_{6.3}Fe_{5.4}Sn_{0.3}]O_{24}$		182		16
$Mn_{6.6}Fe_{10.8}Sn_{0.6}O_{24}$ (4)	$(Mn_{4.8}Fe_{1.2})[Mn_{1.8}Fe_{9.6}Sn_{0.6}]O_{24}$		85		16
$Mg_{6.6}Fe_{10.8}Sn_{0.6}O_{24}$ (5)	$(Mg_{1.92}Fe_{4.08})[Mg_{4.68}Fe_{6.72}Sn_{0.6}]O_{24}$		48		16
$Co_{17.88}Sn_{0.12}O_{24}$ (6)	$(Co_6)[Co_{0.12}Co^{3+}_{11.76}Sn_{0.12}]O_{24}$		8		17
$Mn_{17.88}Sn_{0.12}O_{24}$ (7)	$(Mn_6)[Mn_{0.12}Mn^{3+}_{11.76}Sn_{0.12}]O_{24}$		46		17
$Li_{3.15}Fe_{14.55}Sn_{0.3}O_{24}$ (8)	$(Fe_6)[Fe_{8.55}Li_{3.15}Sn_{0.3}]O_{24}$		125		16
$Ni_{6.6}Fe_{11.1}Sb_{0.3}O_{24}$ (9)	$(Ni_{6x}Fe_{6-6x})[Ni_{6.6-6x}Fe_{5.1+6x}Sb_{0.3}]O_{24}$[b]	308	251	126	12
$Ni_{7.2}Fe_{10.1}Sb_{0.6}O_{24}$ (10)	$(Ni_{6x}Fe_{6-6x})[Ni_{7.2-6x}Fe_{4.2+6x}Sb_{0.6}]O_{24}$[b]	303	235	164	12
$Ni_{8.4}Fe_{8.4}Sb_{1.2}O_{24}$ (11)	$(Ni_{6x}Fe_{6-6x})[Ni_{8.4-6x}Fe_{2.4+6x}Sb_{1.2}]O_{24}$[b]	291	218	148	12
$Ni_{10}Fe_6Sb_2O_{24}$ (12)	$(Ni_{6x}Fe_{6-6x})[Ni_{10-6x}Fe_{6x}Sb_2]O_{24}$[b]	263	193	143	12
$Ni_{10}Fe_6Sb_2O_{24}$ (13)	$(Ni_{1.17}Fe_{4.83})[Ni_{8.83}Fe_{1.17}Sb_2]O_{24}$	263	193	143	this work
$Co_{6.6}Fe_{10.92}Sb_{0.36}O_{24}$ (14)	$(Co_{1.45}Fe_{4.55})[Co_{5.15}Fe_{6.37}Sb_{0.36}]O_{24}$		172 (±63)[c]		19
$Co_{7.26}Fe_{10.08}Sb_{0.72}O_{24}$ (15)	$(Co_{1.89}Fe_{4.11})[Co_{5.37}Fe_{5.97}Sb_{0.72}]O_{24}$		165 (±60)[c]		19
$Co_{12}Fe_3Sb_3O_{24}$ (16)	$(Co_4Fe_2)[Co_8FeSb_3]O_{24}$	263	203	143	this work
$Co_3Ni_9Fe_3Sb_3O_{24}$ (17)	$(Co_3Ni_{0.67}Fe_{2.33})[Ni_{8.33}Fe_{0.67}Sb_3]O_{24}$	287	195	140	this work
$Mg_3Ni_9Fe_3Sb_3O_{24}$ (18)	$(Mg_3Ni_{0.70}Fe_{2.30})[Ni_{8.30}Fe_{0.70}Sb_3]O_{24}$		139	53	this work
$Mg_6Ni_6Fe_3Sb_3O_{24}$ (19)	$(Mg_{3.80}Fe_{2.20})[Ni_6Mg_{2.20}Fe_{0.80}Sb_3]O_{24}$		126	38	this work
$Li_3Co_9Fe_3Te_3O_{24}$ (20)	$(Co_4Fe_2)[Co_5FeLi_3Te_3]O_{24}$		95		18
$Li_3Ni_9Fe_3Te_3O_{24}$ (21)	$(Ni_4Fe_2)[Ni_5FeLi_3Te_3]O_{24}$		85		18

[a] Unless indicated otherwise, the magnesium, manganese, cobalt, and nickel cations are divalent, the iron is trivalent, the tin is tetravalent, the antimony is pentavalent, and the tellurium is hexavalent. [b] The value of x is ca. 0.2. [c] Width of the field distribution.

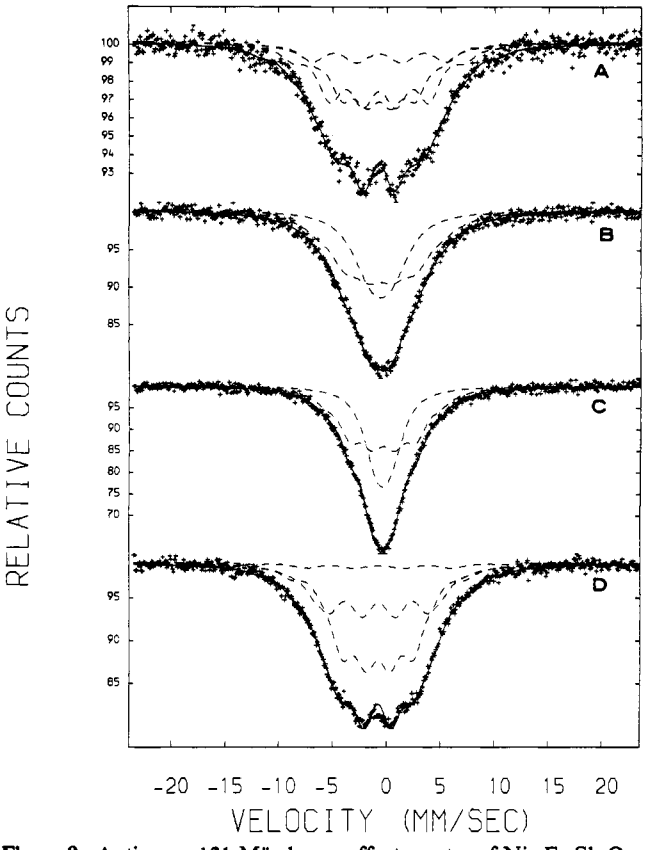

Figure 9. Antimony-121 Mössbauer-effect spectra of $Ni_{10}Fe_6Sb_2O_{24}$ (A), $Mg_3Ni_9Fe_3Sb_3O_{24}$ (B), $Mg_6Ni_6Fe_3Sb_3O_{24}$ (C), and $Co_3Ni_9Fe_3Sb_3O_{24}$ (D) obtained at 4.2 K. The solid lines are the result of a least-squares fit described in the text.

our resulting hyperfine parameters are virtually identical with the earlier results as obtained by method I.[12] Evans has indicated the possibility of ordering of the ions on the A and B sites in $Ni_{10}Fe_6Sb_2O_{24}$ to account for the different supertransferred hyperfine fields observed in this compound, but no such order has been observed by the X-ray diffraction techniques.[3]

Analysis of the Supertransferred Hyperfine Field. In insulator-type spinel oxides, six mechanisms for the transfer of electron spin density to diamagnetic ions such as antimony(V) have been described by Evans[12] and Evans and Swartzendruber.[14] As indicated by these authors, only two of these mechanisms are effective in spinels; the other four may be excluded for different reasons that will not be discussed here.

In the first of these mechanisms, there is a transfer of one electron from the tetrahedral A-site iron(III) ion to the 5s orbital of antimony(V) through the covalent portion of the A–O–B bonding. This transfer corresponds to the configuration change Fe^{3+}–O^{2-}–$Sb^{5+} \rightarrow Fe^{4+}$–$O^{2-}$–$Sb^{4+}$. During this transfer the electron spin direction is maintained and remains antiparallel to the bulk magnetization of the compound. From a measurement[14] of the sign of the hyperfine field on antimony(V), it was concluded that the hyperfine field is antiparallel to the direction of magnetization. This transfer mechanism is thus quite effective, and the role of the tetrahedral A-site cation is predominant. The second possible mechanism involves the overlap of the polarized 2s and 2p electrons of the oxide ion with the 1s, 2s, 3s, and 4s core orbitals of the antimony(V) ion. Because each of these mechanisms for spin transfer involves the bridging oxide ion, the hyperfine field on the antimony(V) is called the supertransferred hyperfine field. Both contributions are represented by the classical expression[15] (1), where β_e is the electron Bohr

$$H_{hyp} = {}^8/_3\pi g\beta_e\langle S_z\rangle[a\phi_{5s}(0) - \sum_{n=1}^{4}\mu_{ns}\phi_{ns}(0)]^2 \qquad (1)$$

magneton, $\langle S_z\rangle$ is the expectation value of the antimony(V) electronic spin, μ_{ns} is the coefficient of the antibonding molecular orbtials for the tetrahedral A-site ion, a is the transfer coefficient from the 3d iron(III) orbital to the 5s antimony(V) orbital, and ϕ_{ns} are the functions for the different core s electrons on the antimony(V). The first term in the brackets in eq 1 represents the first mechanism discussed above and the second term the second mechanism.

Because the computation of antimony(V) wave functions is very difficult, we shall compare the supertransferred hy-

(14) Evans, B. J.; Swartzendruber, L. J. *Phys. Rev. B: Solid State* **1972**, *6*, 223.
(15) Huang, N. L.; Orbach, R.; Simanek, E.; Owen, J.; Taylor, D. R. *Phys. Rev.* **1967**, *156*, 383.
(16) Bokov, V. A.; Novikov, G. V.; Saksonov, Y. G.; Thrukhtanov, V. A.; Yushchuk, S. I. *Sov. Phys.—Solid State (Engl. Transl.)* **1975**, *16*, 2364.
(17) Sekizawa, H.; Okada, T.; Ambe, F. *Physica B+C (Amsterdam)* **1977**, *86–88B+C*, 963.
(18) Gérard, A.; Grandjean, F.; Flêbus, C. *Mat. Res. Soc. Symp. Proc.* **1981**, 495.

perfine fields on tin(IV), antimony(V), and tellurium(VI) in various different spinels. In each case the mechanisms for spin transfer are identical. Table V presents all the measured values for the supertransferred hyperfine fields at these ions from the literature and from this work. Because the nature of the ions in the tetrahedral A site is very important, we have listed the cation distribution for each compound.

Several general conclusions may be drawn from the results presented in Table V. First, in spinels where the A site is exclusively occupied by iron(III) (compounds **1–3** and **8** in Table V), a large hyperfine field on tin(IV) is observed. If the A site contains ions such as manganese(II), cobalt(II), or magnesium(II) (**4–7**) with smaller magnetic moments than iron(III), then the hyperfine field on tin(IV) is considerably smaller. Second, the supertransferred hyperfine field at tin(IV) and antimony(V) may be compared in compounds **2** and **9–13** and in **3** and **14–17**, a comparison that is more straightforward than that of Evans and Swartzendruber.[14] We may compare the largest fields measured on antimony(V) and tin(IV), fields that in both cases result from only iron(III) as neighbors on the tetrahedral A site. It is clear that the antimony(V) supertransferred fields are larger than the tin(IV) fields. This leads to the approximate ratio

$$\frac{H_{hyp}^{Sb(V)}(\mathbf{9})}{H_{hyp}^{Sn(IV)}(\mathbf{2})} = \frac{308}{250} = 1.23$$

in agreement with the 1.3 value calculated by Evans and Swartzendruber[14] and slightly lower than the experimental value of 1.5 quoted by these authors. For compounds **3** and **14**, the similar ratio

$$\frac{H_{hyp}^{Sb(V)}(\mathbf{14})}{H_{hyp}^{Sn(IV)}(\mathbf{3})} = \frac{235}{182} = 1.29$$

is obtained. It is more difficult to compare **3** with **16** and **17** because we do not know the field on an antimony(V) ion that has no cobalt(II) ions as neighbors on the A site. However, the values observed are in the range of the fields found[19] in compounds **14** and **15**. Finally, compounds **8**, **20**, and **21**, each of which contains lithium(I) on their B site, show rather similar fields, but the fields on tellurium(VI) are clearly the smallest observed. From a comparison of compounds **1** and **8**, it is obvious that lithium considerably reduces the supertransferred field on tin(IV). The hyperfine fields measured in the lithium-containing spinels seem to be difficult to explain.[19]

In order to interpret the ratio given above, we must consider the relative importance of both contributions described above to the supertransferred field. As noted by Evans and Swartzendruber,[14] the radial distribution of the *n*s core wave function of tin(IV) is larger than that of antimony(V). Therefore, if the overlap was as important as the covalent spin/charge transfer into the 5s orbital, the hyperfine field at tin(IV) should be at least equal to or larger than that at antimony(V). The difference in hyperfine fields on these ions arises mainly from differences in local bonding properties involving the 5s orbital. Because the presence of iron(III) on the A site seems to influence the supertransferred hyperfine field, we shall consider the transfer of one electron between iron(III) and tin(IV), antimony(V), or tellurium(VI). Thus, we have for each ion in the following configurations:

Sn	I	Sn^{4+}-O^{2-}-Fe^{3+}	
	II	Sn^{3+}-O^{2-}-Fe^{4+}	$E_I - E_{II} = 14$ eV
Sb	I	Sb^{5+}-O^{2-}-Fe^{3+}	
	II	Sb^{4+}-O^{2-}-Fe^{4+}	$E_I - E_{II} = -1$ eV
Te	I	Te^{6+}-O^{2-}-Fe^{3+}	
	II	Te^{5+}-O^{2-}-Fe^{4+}	$E_I - E_{II} = -17$ eV

(19) Evans, B. J. *A. I. P. Conf. Proc.* **1974**, *No. 18*, 518.

The energy differences[14] between these configurations indicate that the ease of electron transfer is in the order tellurium > antimony > tin. The fields should then increase from tin to tellurium in contrast to what is observed. If, on the other hand, the supertransferred hyperfine fields are entirely due to the 3d orbital to 5s orbital electron transfer, then we have the ratio

$$\frac{H_{hyp}^{Sb}}{H_{hyp}^{Sn}} = \frac{[\langle S_z\rangle a^2|\phi_{5s}(0)|^2]_{Sb}}{[\langle S_z\rangle a^2|\phi_{5s}(0)|^2]_{Sn}}$$

where $|\phi_{5s}(0)|^2$ is the 5s electron density at the nucleus. In this expression, we shall assume that $\langle S_z\rangle_{Sb}/\langle S_z\rangle_{Sn} = 1$. Indeed, it measures the degree of spin polarization of the transferred charge and is determined by the magnetic environments. The interatomic distances and angles are very similar in all the compounds studied, but the moments and the number of magnetic neighbors of Sb, Sn, or Te vary slightly from one compound to another. Nevertheless, we think that this should not influence very strongly the degree of spin polarization of the transferred charge, and furthermore, this assumption was used and found to be valid by Evans and Swartzenruber[14] for a comparison of other compounds. Finally, this is the simplest assumption to make, and as we shall see, it gives satisfactory results. The values of $|\phi_{5s}(0)|^2$ have been computed for the free ions,[20] and the following results have been obtained:

$\|\phi(0)\|^2$	Sn	Sb	Te
$5s^1$	51.9	64.9	81.5

Thus, we obtain

$$\frac{|\phi_{5s}(0)|_{Sb}^2}{|\phi_{5s}(0)|_{Sn}^2} = 1.25 \qquad \frac{|\phi_{5s}(0)|_{Te}^2}{|\phi_{5s}(0)|_{Sn}^2} = 1.57$$

Then, if we assume that the transfer parameter is the same for antimony and tin, we may conclude that

$$\frac{H_{hyp}^{Sb}}{H_{hyp}^{Sn}} = \frac{|\phi_{5s}(0)|_{Sb}^2}{|\phi_{5s}(0)|_{Sn}^2} = 1.25$$

a conclusion in good agreement with the experimental ratio given above. Consequently, the relative values of the hyperfine fields on Sn and Sb may be understood on the basis of the relative densities of the 5s electrons at the nucleus. For tellurium(VI), if $a_{Te} = a_{Sb} = a_{Sn}$, the supertransferred hyperfine fields should be larger than for antimony(V) and tin(IV). This is contrary to the observed results. Several reasons may account for this disagreement. (1) There is a large amount of nickel(II) or cobalt(II) on the A site in compounds **18** and **19** that decreases the supertransferred hyperfine field when compared to compound **8**. Furthermore, the presence of Li on the B site may explain a lower field. (2) The supertransferred hyperfine field at 78 K is not saturated. The saturated value would be about 105 kOe. (3) The charge-transfer parameter, a_{Te}, is smaller than a_{Sb} and a_{Sn}. However, this is contrary to expectation. (4) The fraction of polarized transferred spin is smaller than for antimony or tin.

For the compounds studied in this paper (**13**, **16–19**), the large amount of antimony on the B sites does not permit a straightforward comparison with the tin compounds. Furthermore, the orthorhombic structure found in compounds **16–19** must be taken into account in the analysis of the supertransferred fields.

For the cubic compound, $Ni_{10}Fe_6Sb_2O_{24}$ (**13**), a good fit to the antimony-121 Mössbauer spectra was obtained with the

(20) Ruby, S. L.; Shenoy, G. K. In "Mössbauer Isomer Shifts"; Shenoy, G. K., Wagner, F. E., Eds.; North-Holland Publishing Co.: Amsterdam, 1978; p 617.

isomer shifts, hyperfine fields, and relative areas very similar to those obtained by Evans.[12] In the spinel structure, each B site has six A-site neighbors, and, because of the random occupation of the A sites by iron(III) and nickel(II) ions, the antimony(V) ions on the B sites may have as many as seven different environments corresponding to zero to six nickel(II) ions on the A sites. The three different observed hyperfine fields (Table IV) account rather well for these different environments. On average in $Ni_{10}Fe_6Sb_2O_{24}$, there are 4.8 iron(III) and 1.2 nickel(II) ions on the six A sites.

In the orthorhombic compounds, **16–19**, antimony(V) may occupy the two different octahedral B sites, 4c and 4b, with the population ratio of 1/2. As in the spinel structure, each antimony(V) has six A-site first neighbors on either the 8h or 4e site, with the average occupations (listed in Table IV) determined by the cationic distribution given in Table I. By taking into account the general relative intensities and the hyperfine field values obtained for each antimony-121 subspectrum, the hyperfine fields found for $Co_{12}Fe_3Sb_3O_{24}$ (**16**), $Co_3Ni_9Fe_3Sb_3O_{24}$ (**17**), $Mg_3Ni_9Fe_3Sb_3O_{24}$ (**18**), and $Mg_6Ni_6Fe_3Sb_3O_{24}$ (**19**) may be assigned to antimony in the 4c and 4b sites as indicated in Table IV.

The difference in the supertransferred hyperfine field on the two antimony sites may be accounted for by the different cation distributions on the first-neighbor tetrahedral A sites. As shown by Evans[12] in $NiFe_2O_4$, the average contribution to the supertransferred hyperfine field per iron(III) ion on an A site is 57 kOe and the total field is decreased by 38 kOe if one of the iron(III) ions is replaced with nickel(II) on the tetrahedral A site as is observed in $Ni_{10}Fe_6Sb_2O_{24}$. Thus, the contribution to the field per nickel(II) ion on an A site is estimated to be ca. 19 kOe. According to Petitt and Forester,[21] the similar substitution of iron(III) with cobalt(II) decreases the field at an iron-57 on the B site by 18 kOe. If we assume the same process for the supertransferred field at antimony, the contribution per cobalt(II) ion on the A site is ca. 39 kOe. A magnesium(II) ion on the A site is assumed to not contribute to the supertransferred hyperfine field. With these assumptions, we may calculate the supertransferred hyperfine field at antimony in each of the compounds under study. The results are given in Table IV. It may be concluded that the order of magnitude of the component field for each ion is correct and that the difference between the 4c and 4b sites is well explained. The variation from compound to compound is also well reproduced. It seems that the estimation of the cobalt(II) contribution may be too large. It is clear that the random distribution of cobalt(II), nickel(II), and iron(III) or magnesium(II), nickel(II), and iron(III) on the 8h site in $Co_3Ni_9Fe_3Sb_3O_{24}$ and $Mg_3Ni_9Fe_3Sb_3O_{24}$ may perturb the calculated hyperfine fields. Finally, the 30-kOe supertransferred hyperfine field at antimony(V) on the 4b site in $Mg_6Ni_6Fe_3Sb_3O_{24}$ may be due either to B-site–B-site magnetic interactions because there are no magnetic ions on the neighboring A sites or to A-site second neighbors occupied by magnetic ions.

Acknowledgment. We are very indebted to Prof. P. Tarte and D. J. Preudhomme for supplying the samples and to Drs. A. Gérard, T. E. Cranshaw, A. K. Cheetham and L. Becker for their assistance and many helpful discussions. G.J.L. thanks NATO, for a cooperative scientific research grant, and the NSF (Grant INT-8202403), both of which supported this work in parts.

Registry No. $Zn_{12}Fe_3Sb_3O_{24}$, 70316-00-6; $Mg_{12}Fe_3Sb_3O_{24}$, 70198-65-1; $Co_{12}Fe_3Sb_3O_{24}$, 70315-94-5; $Co_3Ni_9Fe_3Sb_3O_{24}$, 70315-91-2; $Mg_3Ni_9Fe_3Sb_3O_{24}$, 70315-99-0; $Mg_6Ni_6Fe_3Sb_3O_{24}$, 70315-98-9; $Ni_{10}Fe_6Sb_2O_{24}$, 12029-12-8; antimony-121, 14265-72-6.

Supplementary Material Available: Table III, giving an analysis of the optimum stoichiometry obtained from ordered Mössbauer-effect spectra (2 pages). Ordering information is given on any current masthead page.

(21) Petitt, G. A., Forester, D. W. *Phys. Rev. B: Solid State* **1971**, *4*, 3912.